Scale Law of Far-Field Thermal Radiation from Plasmonic Metasurfaces

Jiayu Li, Bowen Yu, and Sheng Shen

Phys. Rev. Lett. **124**, 137401 — Published 31 March 2020

DOI: 10.1103/PhysRevLett.124.137401

Scale law of far-field thermal radiation from plasmonic metasurfaces

Jiayu Li, Bowen Yu, Sheng Shen*

Department of Mechanical Engineering, Carnegie Mellon University, Pittsburgh, PA 15213 USA

*Corresponding author. E-mail: sshen1@cmu.edu.

Abstract

Although metamaterials or metasurfaces consisting of patterned subwavelength structures have been widely employed for thermal emission control, the collective behavior of the emitter arrays in a metasurface still remains unclear. Here, based on quasi-normal mode theory, we derive a new scale law to elucidate the far-field thermal emission from a metasurface composed of densely packed plasmonic nanoemitters. The tight binding method is used to approximate the collective resonant mode of the emitter array. Due to in-phase near-field interaction, the thermal radiation from a single emitter in a metasurface is suppressed by its adjacent emitters. We find that the overall far-field thermal radiation from a metasurface can be either positively or negatively correlated with the packing density of the emitters, depending on the mode properties of the single emitter. This new scale law thus serves as a general guideline for designing metasurfaces with desired thermal emission properties.

Thermal radiation, which physically originates from the electromagnetic waves emitted from thermally induced random currents in materials, plays a vital role in many fields, such as energy conversion [1–6], infrared sensing[7,8], radiative cooling[9–14] and thermal management[15–18]. In recent years, metasurfaces consisting of an array of subwavelength plasmonic thermal emitters have emerged as an important platform to actively control and manipulate far-field thermal radiation[19–27]. Although the far-field thermal radiation from a single plasmonic thermal emitter is well comprehended under the framework of Quasi-normal mode (QNM) theory[20,28] and coupled mode theory[29,30], the collective behavior of the closely packed nanoscale plasmonic emitters in a metasurface remains largely unknown.

Here we develop a new scale law to predict and design the thermal emission from a metasurface based on QNM theory and the tight-binding (TB) method. In this new theory, the thermal emission from one individual sub-wavelength emitter in a metasurface is described by QNM theory, whereas the TB method is employed to quantify the red shift of the thermal emission spectrum due to the interactions between the emitters. Based on this new scale law, we can quantitatively describe the suppression of thermal emission from a single plasmonic emitter when coupled with adjacent emitters in the same phase. We find that depending on the QNM properties of a single emitter, the overall far-field thermal radiation from the metasurface can be either positively or negatively correlated with the packing density of the emitters. We also experimentally verify the new scale law by fabricating and measuring plasmonic metasurfaces made by gold nanorods. Hence, this new scale law could perform as a general theoretical framework for designing metasurfaces with desired thermal emission properties, which has important implications in thermal energy conversion, thermal management and infrared sensing.

QNMs, which are the eigen solutions to the source free Maxwell equation in the non-Hermitian system[31–33], were introduced to quantitatively describe the thermal radiation from a single plasmonic thermal emitter. The TB method was first introduced to calculate the electronic band structure based upon the superposition of wave functions for isolated atoms[34,35]. Here we adopt the same methodology to account for the modification of the single emitter's QNM inside the array, provided that the electric field of a plasmonic emitter is highly confined around its surface. Due to the translational symmetry of the plasmonic emitter array in a metasurface (FIG. 1), the collective QNM of the entire emitter array should follow the form of Bloch's wave. Therefore, the QNM is a periodic function of the lattice constant of the emitter array $\boldsymbol{R}_l = l_x P_x \hat{\boldsymbol{e}}_{\boldsymbol{x}} + l_y P_y \hat{\boldsymbol{e}}_{\boldsymbol{y}}$, which are $\boldsymbol{E_n}(\omega(\boldsymbol{k}), \boldsymbol{r}) = \frac{1}{\sqrt{N}} \sum_l \boldsymbol{a_n}(\boldsymbol{R_l}, \boldsymbol{r}) e^{i\boldsymbol{k}\cdot\boldsymbol{R_l}}$, $\boldsymbol{H_n}(\omega(\boldsymbol{k}), \boldsymbol{r}) = \frac{1}{\sqrt{N}} \sum_l \boldsymbol{b_n}(\boldsymbol{R}_l, r) e^{i\boldsymbol{k}\cdot\boldsymbol{R_l}}$. l_x and l_y here are the integers. *N* is the number of emitters considered. The coefficients $\boldsymbol{a_n}(\boldsymbol{R}_l, \boldsymbol{r})$ and $\boldsymbol{b_n}(\boldsymbol{R}_l, \boldsymbol{r})$ are two sets of Wannier functions which only depend on $\boldsymbol{r} - \boldsymbol{R}_l$.

Since the QNM of a plasmonic emitter is highly confined around its surface, we assume that the QNM of the entire emitter array behaves similarly in the vicinity of each emitter as it does in the case of a standalone single emitter. Therefore we can use the QNM of a single emitter $\{\boldsymbol{e}_n(\omega_n, \boldsymbol{r}), \boldsymbol{h}_n(\omega_n, \boldsymbol{r})\}$ as the approximation of $\boldsymbol{a_n}(\boldsymbol{r} - \boldsymbol{R}_l)$ and $\boldsymbol{b_n}(\boldsymbol{r} - \boldsymbol{R}_l)$, namely: $\boldsymbol{E}_n(\omega(\boldsymbol{k}), \boldsymbol{r}) = \frac{1}{\sqrt{N}} \sum_l \boldsymbol{e}_n(\omega_n, \boldsymbol{r} - \boldsymbol{R}_l) e^{i\boldsymbol{k}\cdot\boldsymbol{R}_l}$, $\boldsymbol{H}_n(\omega(\boldsymbol{k}), \boldsymbol{r}) = \frac{1}{\sqrt{N}} \sum_l \boldsymbol{h}_n(\omega_n, \boldsymbol{r} - \boldsymbol{R}_l) e^{i\boldsymbol{k}\cdot\boldsymbol{R}_l}$. Here, $\{\boldsymbol{e}_n(\omega_n, \boldsymbol{r}), \boldsymbol{h}_n(\omega_n, \boldsymbol{r})\}$ is the solution to the source free Maxwell equation for a stand-alone emitter:

$$\begin{aligned} \nabla \times \boldsymbol{e}_n(\omega_n, \boldsymbol{r}) &= i\omega_n \mu_0 \boldsymbol{h}_n(\boldsymbol{r}) \\ \nabla \times \boldsymbol{h}_n(\omega_n, \boldsymbol{r}) &= -i\omega_n \varepsilon_s(\omega_n, \boldsymbol{r}) \boldsymbol{e}_n(\boldsymbol{r}) \ , \end{aligned} \tag{1}$$

where $\varepsilon_s(\omega_n, \boldsymbol{r})$ is the permittivity function for the emitter. In order to satisfy the boundary conditions of Maxwell's equation, the coefficients of the Bloch-form QNM of the metasurface should be modified as the following form: $\tilde{\boldsymbol{e}}_{\boldsymbol{n}}(\omega_n, \boldsymbol{r}-\boldsymbol{R}_l) = \boldsymbol{e}_n(\omega_n, \boldsymbol{r}-\boldsymbol{R}_l)\gamma(\omega_n, \boldsymbol{r}-\boldsymbol{R}_l)$, $\tilde{\boldsymbol{h}}_{\boldsymbol{n}}(\omega_n, \boldsymbol{r}-\boldsymbol{R}_l) = \boldsymbol{h}_n(\omega_n, \boldsymbol{r}-\boldsymbol{R}_l)\gamma(\omega_n, \boldsymbol{r}-\boldsymbol{R}_l)$, where $\gamma_{\omega_n,l} = \gamma(\omega_n, \boldsymbol{r}-\boldsymbol{R}_l) = 1/\sum_l \varepsilon_s(\omega_n, \boldsymbol{r}-\boldsymbol{R}_l)$ and ε_s here is defined inside the repeating unit cell indexed by the lattice constant (l_x, l_y). Thus, the new Bloch-form QNM satisfies the continuous boundary conditions at the interface of the emitter and the background material.

Substituting the QNM of the entire emitter array into the source-free Maxwell equation $\nabla \times \boldsymbol{H}_n(\boldsymbol{r}) = -i\omega(\boldsymbol{k})\varepsilon_t(\omega(\boldsymbol{k}), \boldsymbol{r})\boldsymbol{E}_n(\boldsymbol{r})$, we have

$$\begin{aligned}
&\sum_l \frac{1}{\sqrt{N}} \nabla \times \boldsymbol{h}_n(\omega_n, \boldsymbol{r}-\boldsymbol{R}_l) e^{i\boldsymbol{k}\cdot\boldsymbol{R}_l} \gamma_{\omega_n,l} \\
&= \frac{1}{\sqrt{N}} \sum_l e^{i\boldsymbol{k}\cdot\boldsymbol{R}_l} \gamma_{\omega_n,l} \left(-i\omega_n \varepsilon_s(\omega_n, \boldsymbol{r}-\boldsymbol{R}_l)\boldsymbol{e}_n(\boldsymbol{r}-\boldsymbol{R}_l)\right) \\
&= \frac{1}{\sqrt{N}} \sum_l -i\omega(\boldsymbol{k})\varepsilon_t(\omega(\boldsymbol{k}), \boldsymbol{r})\boldsymbol{e}_n(\omega_n, \boldsymbol{r}-\boldsymbol{R}_l) e^{i\boldsymbol{k}\cdot\boldsymbol{R}_l} \gamma_{\omega_n,l} \ .
\end{aligned} \tag{2}$$

Note that $\varepsilon_t(\omega(\boldsymbol{k}), \boldsymbol{r})$ is the permittivity function of the emitter array which is related to the single emitter permittivity function by $\varepsilon_t(\omega, \boldsymbol{r}) = \sum_l \varepsilon_s(\omega, \boldsymbol{r}-\boldsymbol{R}_l)$. Now we obtain the new equation between the modified resonant frequency $\omega(\boldsymbol{k})$ and the resonant frequency of the single emitter ω_n:

$$\sum_l e^{i\boldsymbol{k}\cdot\boldsymbol{R}_l} \gamma_{\omega_n,l} \omega_n \varepsilon_s(\omega_n, \boldsymbol{r}-\boldsymbol{R}_l)\boldsymbol{e}_n(\omega_n, \boldsymbol{r}-\boldsymbol{R}_l) = \sum_l e^{i\boldsymbol{k}\cdot\boldsymbol{R}_l} \gamma_{\omega_n,l} \omega(\boldsymbol{k})\varepsilon_t(\omega(\boldsymbol{k}), \boldsymbol{r})\boldsymbol{e}_n(\omega_n, \boldsymbol{r}-\boldsymbol{R}_l). \tag{3}$$

Multiplying both sides of Equation (3) with $\boldsymbol{e}_n(\omega_n, \boldsymbol{r}-\boldsymbol{R}_{l'})$ and integrating over the whole emitter array volume, we get:

$$\sum_l \int dr^3 e^{i\boldsymbol{k}\cdot\boldsymbol{R}_l}\gamma_{\omega_n,l}\omega_n\varepsilon_s(\omega_n,\boldsymbol{r}-\boldsymbol{R}_l)\boldsymbol{e}_{n,l}\boldsymbol{e}_{n,l'} = \sum_l \int dr^3 e^{i\boldsymbol{k}\cdot\boldsymbol{R}_l}\omega(\boldsymbol{k})\gamma_{\omega_n,l}\varepsilon_t(\omega(\boldsymbol{k}),\boldsymbol{r})\boldsymbol{e}_{n,l}\boldsymbol{e}_{n,l'} \ , \tag{4}$$

where $\boldsymbol{e}_{n,l} = \boldsymbol{e}_n(\omega_n, \boldsymbol{r}-\boldsymbol{R}_l)$. If the distance between adjacent emitters is not significantly smaller than the lateral dimension of the emitters and the index l' is set to be (0,0) or $\boldsymbol{0}$, then the left-hand side (LHS) of Equation (4) is reduced to $\sum_l \int dr^3 e^{i\boldsymbol{k}\cdot\boldsymbol{R}_l}\gamma_{\omega_n,l}\omega_n\varepsilon_s(\omega_n,\boldsymbol{r}-\boldsymbol{R}_l)\boldsymbol{e}_{n,l}\boldsymbol{e}_{n,l'} = \int dr^3\gamma_{\omega_n,0}\omega_n\varepsilon_s(\omega_n,\boldsymbol{r})\boldsymbol{e}_{n,\boldsymbol{0}}\boldsymbol{e}_{n,\boldsymbol{0}}$. Finally, the modified resonant QNM frequency of the emitter array can be calculated by solving the equation:

$$\sum_l \int dr^3 e^{i\boldsymbol{k}\cdot\boldsymbol{R}_l}\gamma_{\omega_n,l}\omega(\boldsymbol{k})\varepsilon_t(\omega(\boldsymbol{k}),\boldsymbol{r})\boldsymbol{e}_{n,l}\boldsymbol{e}_{n,l'} = \int dr^3\gamma_{\omega_n,0}\omega_n\varepsilon_s(\omega_n,\boldsymbol{r})\boldsymbol{e}_{n,\boldsymbol{0}}\boldsymbol{e}_{n,\boldsymbol{0}} \ . \tag{5}$$

The index l only needs to run over the nearby emitters to obtain the accurate result. If we only consider the coupling effect from the nearest emitters, the modified resonant frequency for the 2D array of emitters in a metasurface can be calculated as follows:

$$\omega(\boldsymbol{k}) = \frac{I_0^s}{I_0^t + 2cos(\boldsymbol{k}\cdot\boldsymbol{R}_0)I_{1,x}^t + 2cos(\boldsymbol{k}\cdot\boldsymbol{R}_0)I_{1,y}^t}\omega_n \ . \tag{6}$$

The integral $I_l^s = \int dr^3 e^{i\boldsymbol{k}\cdot\boldsymbol{R}_l}\gamma_{\omega_n,l}\varepsilon_s(\omega_n,\boldsymbol{r})e_{n,\boldsymbol{0}}e_{n,l}$, $I_l^t = \int dr^3 e^{i\boldsymbol{k}\cdot\boldsymbol{R}_l}\gamma_{\omega_n,l}\varepsilon_t(\omega(\boldsymbol{k}),\boldsymbol{r})e_{n,\boldsymbol{0}}e_{n,l}$. The integral $I_{1,x}^t$ and $I_{1,y}^t$ are mode overlapping terms from the adjacent emitters in the x-direction and y-direction respectively. Equation (6) could be solved iteratively. If the mode overlapping terms $I_{1,x}^t$ and $I_{1,y}^t$ are small as compared to the zero-order coupling term I_0^t, then $\omega(\boldsymbol{k}) = \omega =$

$\omega_n I_0^s / I_0^t$. In this case, the resonant frequency has no dispersion with respect to the lattice momentum $\boldsymbol{k}$.

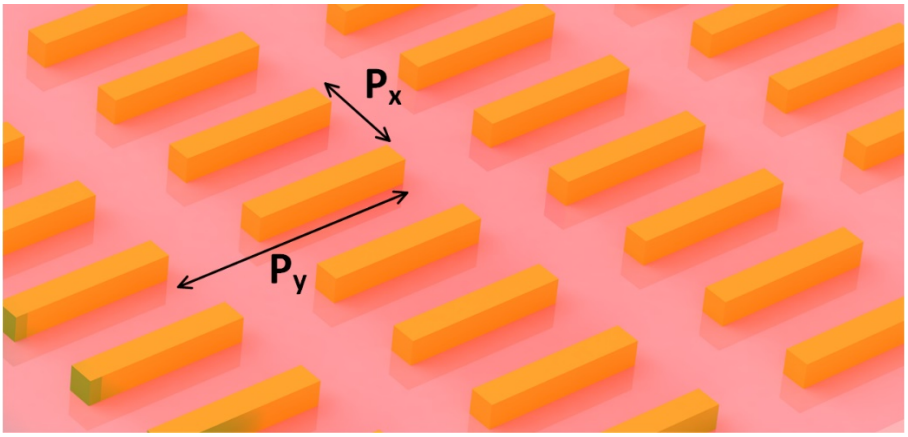

FIG. 1. Schematic of an array of resonant thermal emitters in a plasmonic metasurface.

For a metasurface made from an array of plasmonic emitters with Px and Py as the periodicities in the x- and y-directions, we assume that there exists a unit cell A including N+1 emitters, where when the center emitter is thermally excited, the rest of N emitters are coupled to it, and the coupling of the emitters outside this unit cell can be neglected. We follow the same mathematical derivation in our previous work[28] to rewrite the far-field thermal radiation from the unit cell. As an approximation, we use the QNM of a single emitter to calculate the coupling strength in the emitter array. The modification of the resonant frequency is addressed by the TB method. We can express the far-field thermal radiation from one emitter inside the array in terms of the fractional losses D_E, D_A and D_∞ from the single emitter's QNM profile yet at the modified resonant frequency ω.

$$\phi_{\infty}(\omega) = 4\left(\frac{D_E}{D_{\infty} + D_E + \sum_{i=1}^{N} D_{A_i}} F\right)\left(P - \frac{D_E + \sum_{i=1}^{N} D_{A_i}}{D_{\infty} + D_E + \sum_{i=1}^{N} D_{A_i}} F\right), \tag{7}$$

where $D_E = \int_{V_E} dr'^3 \frac{1}{2}\sigma_E \mathrm{Re}(\omega)\left|E(r')\right|^2$, $D_{\infty} = \int_{\partial V} dr^2 \frac{1}{2}\mathrm{Re}\left(E(r)\times H^{\dagger}(r)\right)$, and $D_{A_i} = \int_{V_{A_i}} dr^3 \frac{1}{2}\sigma_{A_i}\mathrm{Re}(\omega)\left|E_{A_i}(r)\right|^2$. P and F are two imperfection factors that each has a value between 0 and 1. Here E_{A_i} is the QNM excited inside the *i*th emitter. $\phi_{\infty}(\omega_0)$ is the reduced heat flow, and the overall radiative heat flux can be estimated as $\Phi_{\infty} = \int \frac{d\omega}{2\pi}\Theta(\omega, T)\left[\frac{1}{A}L(\omega)\phi_{\infty}(\omega_0)\right]$, where $\Theta(\omega, T)$ is the Planck term, $L(\omega)$ is the Lorentzian lineshape function $L_n(\omega) = \frac{Im(\omega_0)^2}{Im(\omega_0)^2 + (Re(\omega_n) - \omega)^2}$ [36]. The relative magnitude of D_E and D_{A_i} is determined by the coupling strength of the center emitter and the *i*th emitter. For two emitters to be coupled, the excitation of the QNM in one emitter needs to effectively invoke the same QNM in the other emitter. To quantitatively investigate the coupling strength between two adjacent emitters placed in the near field, we can integrate the QNM field overlapping as

$f_n(r) = \int dr'^3 E_0(r')^{\dagger} E_n(r' - r_n) / \int dr'^3 E_0(r')^{\dagger} E_0(r')$, where E_0 and $E_n$are the electrical fields of the QNMs of the center emitter and the nth emitter respectively, and r_n is the location of the *n*th emitter center. Thus, the relative intensity of the QNM field incurred inside the neighboring emitters can be evaluated. We further introduce the effective number of emitters coupled

$$N_{eff} = \sum_{n=1}^{N} f_n(r)$$

(8)

to calculate the far-field thermal radiation from one emitter in the array.

Under the electric quasi-static approximation for a plasmonic emitter, the imperfection factors P and F approach unity[28]. By utilizing the effective number of emitters coupled, we can get $\sum_i D_{A_i} = N_{eff} D_E$. Finally, the far-field thermal radiation from one emitter inside the array becomes

$$\phi_\infty(\omega) = \frac{4 D_E D_\infty}{\left(\left(N_{eff}+1\right) D_E + D_\infty\right)^2} = \frac{4\beta}{\left(\left(N_{eff}+1\right)\beta + 1\right)^2},$$

(9)

where $\beta = \frac{D_E}{D_\infty}$. Depending on the coupling strength of the plasmonic emitters, there exist three types of scaling behaviors for the far-field thermal radiation as follows. (i) When the plasmonic emitters are in the overcoupling regime[37,38], the QNMs of individual emitters are in the same phase and intensity. Hence N_{eff} approaches N as indicated by Equation (8), and the total thermal radiation from (N+1) such plasmonic emitters inside the unit cell is $\phi_{\infty,total}(\omega) = \frac{4(N+1)\beta}{((N+1)\beta+1)^2} \propto \frac{1}{N+1}$. Thus, it indicates that the total thermal radiation from overcoupled plasmonic emitter array will be inversely proportional to the packing density. (ii) When the plasmonic emitters are in the non-coupling regime, the QNMs of individual emitters are in uncorrelated phase, hence N_{eff} becomes 0. The total thermal radiation from such an uncoupled plasmonic emitter array is $\phi_{\infty,total}(\omega) = \frac{4(N+1)\beta}{(\beta+1)^2} \propto (N+1)$. This implies that the total thermal radiation is now proportional to the packing density of the plasmonic emitter array. (iii) When the coupling between adjacent plasmonic emitters leads to the opposite phase for their QNMs, N_{eff} could become a negative value (see Supplemental Materials), and the total thermal radiation from such a plasmonic emitter array is

able to deliver superior power as compared to the conventional uncoupled plasmonic emitter array[37,38]: $\phi_{\infty,total}(\omega) = \frac{4(N+1)\beta}{\left((N_{eff}+1)\beta+1\right)^2} > \frac{4(N+1)\beta}{(\beta+1)^2} = (N+1)\phi_{\infty,uncoupled}$. It should be noted that the cases in (i) and (iii) arrive at the same scaling behaviors as reported in the previous work[37], which are referred to as the "superradiance" and "subradiance" effects, respectively. For the cases other than the aforementioned three scenarios, the thermal radiation from one emitter inside the array is always suppressed, compared with the thermal radiation from the stand-alone single emitter, $\frac{4\beta}{(\beta+1)^2}$ (see Supplemental Materials). As the distance between adjacent emitters decreases, the thermal emission from one emitter inside the array ϕ_∞ is continuously suppressed, while the packing density increases simultaneously. If the decreasing rate of ϕ_∞ is larger than the increasing rate of the packing density, the total thermal radiation from the unit cell will be positively correlated with the packing density. Otherwise, the total thermal radiation will be negatively correlated with the packing density.

To verify this new scale law, we theoretically and experimentally investigate the far-field thermal radiation from metasurfaces consisting of gold nanorod arrays. Each nanorod emitter has a rectangular shape with 2.5 microns in length, and 70 nm by 80 nm in cross-section area. In the experiment, the nanorod emitter array is placed on a substrate which is designed to reflect all the infrared radiation to the upper space for the measurement purpose. The substrate is composed of a 150 nm thick alumina layer and a 50nm thick aluminum layer deposited on a SiO_2 thermal oxide wafer. The spatial distribution function of the electrical field intensity around a single nanorod emitter with and without the substrate is plotted in Fig. 2(a) for the first resonance frequency, and the corresponding QNM field profile is shown in the inset of Fig. 2(a). The exponential decay of

electric field intensity leads to a fast-descending coupling strength and effective number of emitters coupled to the center one with respect to the distance between adjacent emitters, as shown in Fig. 2(b). The coupling strength can vary when emitters are aligned in different directions. In this case, the coupling strength in the x-direction (shoulder-to-shoulder) is stronger than that in the y-direction (head-to-head) because of the dipole-like QNM profile. Also, the coupling strength is weakened when the emitter is placed on the high-index substrate as shown by the blue curve in Fig. 2(a). The weak coupling makes it difficult to observe the subradiance effect or reach the superradiance limit. For this QNM, the value of β is calculated to be 0.11 by the frequency-domain finite element method, and the reduced radiative heat flow ϕ_∞ at the resonant frequency from the stand-alone nanorod emitter is 0.36. By normalizing to the blackbody limit[28] $\Phi_{BB} = \int \frac{d\omega}{2\pi} \Theta\left(\frac{2\pi}{\lambda^2}\right)$, the emissivity of the metasurface at the resonant frequency can be calculated.

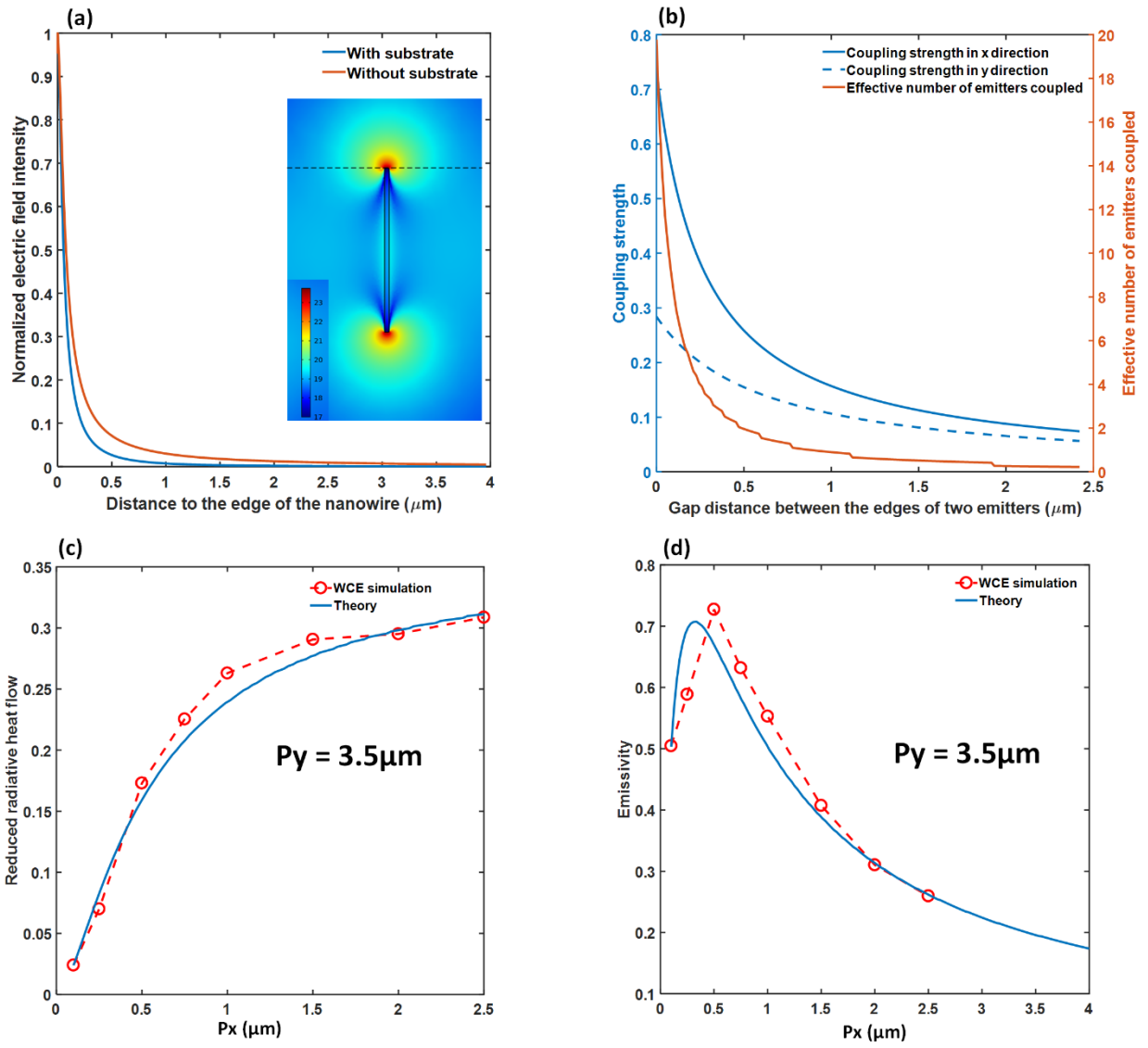

FIG. 2. (a) Electric field intensity around a single nanowire emitter with and without the substrate. Inset: corresponding QNM field profile. (b) Coupling strengths between two emitters in the x- and y-directions, and corresponding effective number of emitters coupled to the emitter due to the x-direction coupling. (c) Thermal emission from a single emitter in the array at Py=3.5 μm but different Px. (d) Corresponding emissivity of the metasurface (gold nanorod array), where the total thermal emission is normalized to blackbody radiation.

Here we first investigate the suspended nanorod emitter array in vacuum where Py = 3.5 μm but Px varies. In Fig. 2(c), the predicted reduced radiative heat flow from one emitter inside the array is plotted in the blue curve. The corresponding emissivity is plotted in Fig. 2(d). The maximum

emissivity of 0.72 is achieved when Px is around 500 nm. To validate our theory, we directly calculate the far-field thermal radiation from the metasurface using the Wiener chaos expansion (WCE) method[22,39]. The direct calculation and the prediction from the new scale law show good agreement, as shown in Figs.2(c) and (d).

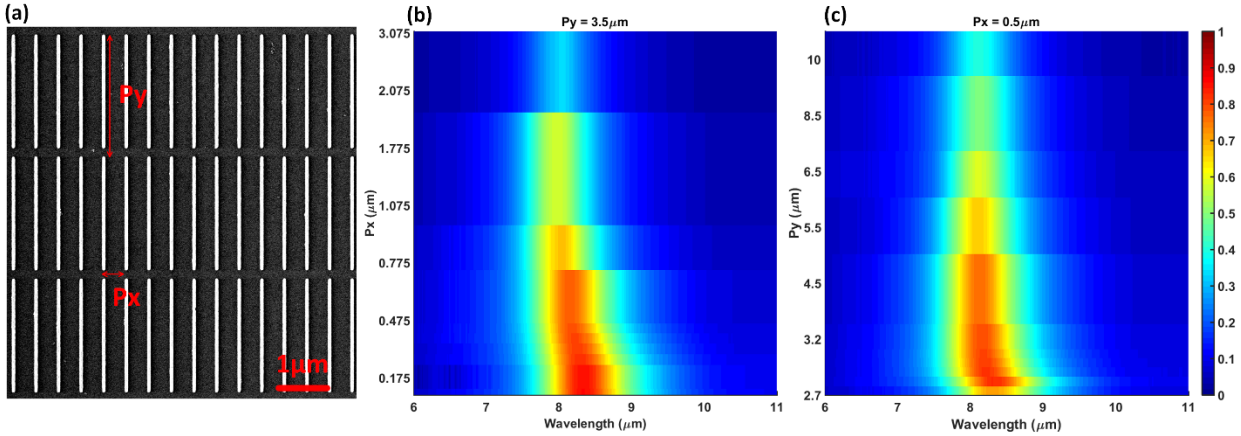

FIG. 3. (a) SEM image of the nanorod emitter array when Py = 2.7μm and Px = 0.5μm. (b) Emission spectra of a nanorod emitter array when Py is fixed to be 3.5μm but Px varies, and (c) when Px is fixed to be 0.5μm but Py varies. The color bar on the right represents the emissivity of the nanorod emitter arrays.

We experimentally measure the emissivity of metasurfaces made from the nanorod emitter arrays, where the emissivity is indirectly evaluated as the absorptivity according to the Kirchhoff's law (see Supplemental Materials). The scanning electron microscopy (SEM) image of the fabricated nanorod emitter arrays is shown in Fig. 3(a). For Py = 3.5 μm, the measured emission spectra with varied Px are plotted in Fig. 3(b). Indeed, the emissivity increases monotonically with the packing density as shown by both the experiment results and the theoretical prediction in Fig. 4(a), and the maximum emissivity point is pushed to be around Px = 100 nm. The overall emissivity is also larger than that without the substrate. The decrease of the mode coupling strength in the existence of a high-index substrate leads to larger thermal emission from the individual emitter at the same

packing density, thereby resulting in a smaller optimized periodicity value and a larger maximum emissivity as compared to the case in vacuum (Fig. 2(d)). There is a red shift of the resonant frequency of the nanorod emitter inside the array when Px decreases (Fig. 4(c)). The new theory developed in this work is utilized to calculate the frequency shifting (Fig. 4(d)). Our experimental results agree well with our new theory.

To reach the "turning point" of the correlation between the metasurface emissivity and the nanorod packing density, we can further increase the coupling strength between the emitters by shrinking the periodicities. Here we use the other nanorod emitter array pattern where Px is fixed to be 0.5 μm such that the coupling in the x-direction is still strong, but Py varies. The corresponding emission spectra are shown in Fig. 3 (c). In Fig. 4(b), an optimized periodicity is found to be around Py = 2.75 μm as predicted by the new scale law. The emissivity of the metasurface keeps increasing with the increased packing density until Py reaches 2.75 μm. After passing the optimized point, the overall emissivity decreases with increasing the packing density. An optimized point reaches at Py = 2.8 μm which gives the emissivity of 0.83. When Py is further reduced, the emissivity quickly decreases. The discrepancies between theory and experiment in Fig. 4 are attributed to the following reasons. First, in QNM theory, we only consider the contribution of dominant resonant modes. The non-resonant component of the radiation field is treated as background noise[36]. Second, the nanorod roughness and the small variations of the nanorod sizes (~20 nm in the length direction and ~5 nm in the width direction) also contribute to the deviation of the theoretical prediction from experimental results.

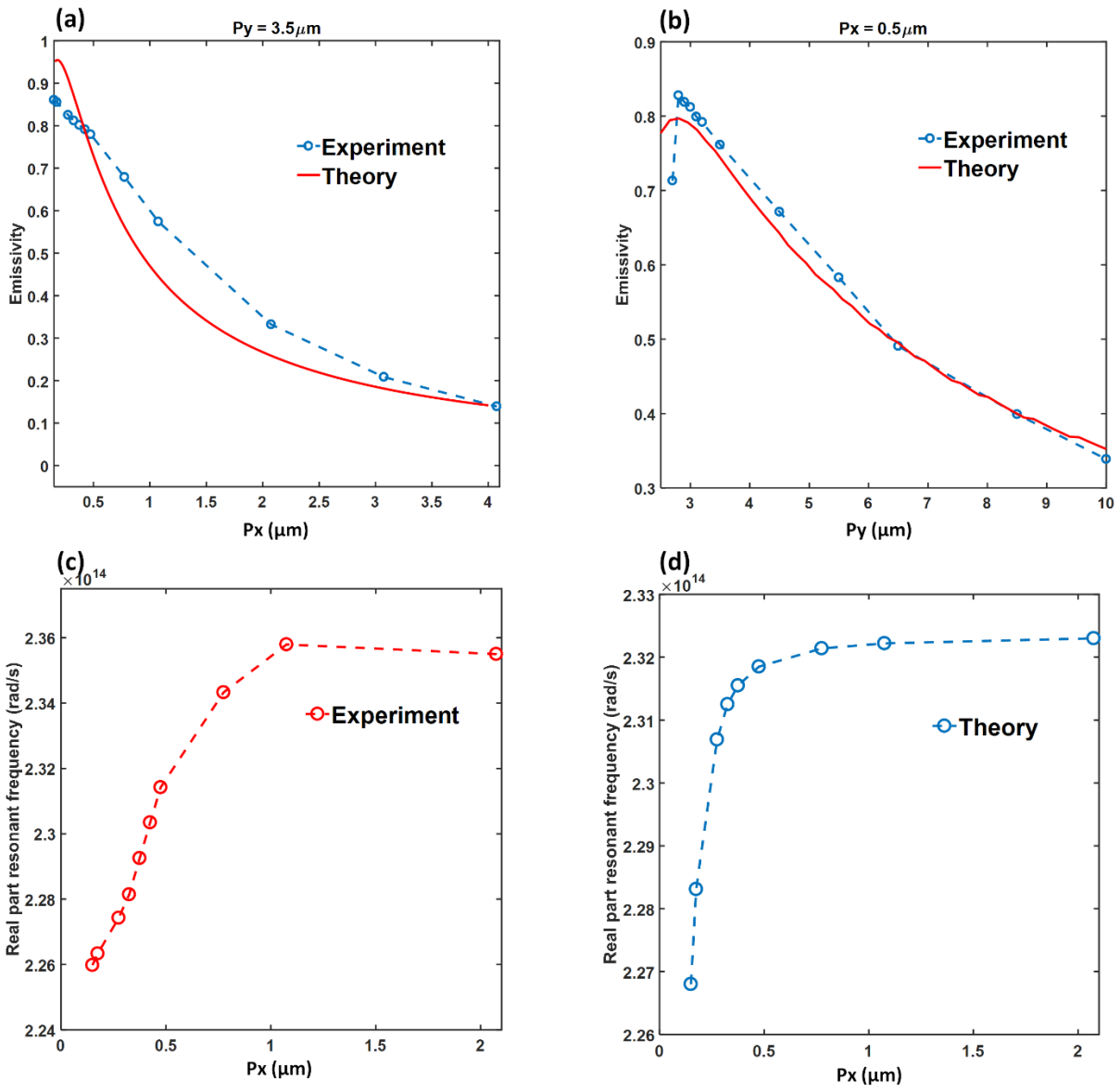

FIG. 4. Emissivity of the nanorod emitter array for (a) Py =3.5μm and (b) Px = 0.5μm. The red shifts of the resonance frequency observed in experiment (c) and predicted by theory (d).

In summary, we develop a new scale law of far-field thermal emission by applying QNM theory to the metasurface consisting of densely packed plasmonic emitters. The TB method is used to approximate the collective resonant mode of the emitter array. The thermal radiation from a single emitter inside the array is observed to be suppressed by its adjacent emitters due to their in-phase

near-field coupling, where such the suppression of thermal radiation can be quantitively predicted by the new scale law. Depending on properties of the single emitter's QNM, the overall thermal radiation can be either positively or negatively correlated with the packing density. This new scale law of thermal radiation can thus serve as a general guideline for designing metasurfaces with desired thermal emission properties.

Acknowledgements

This work was primarily supported by the Defense Threat Reduction Agency (Grant no. HDTRA11910028). The content of the information does not necessarily reflect the position or the policy of the federal government, and no official endorsement should be inferred. This work was funded partially by the Dowd Fellowship from the College of Engineering at Carnegie Mellon University.

References

[1] S. Basu, Z.M. Zhang, and C.J. Fu, Int. J. Energy Res. **33**, 1203 (2009).

[2] M. Laroche, R. Carminati, and J.-J. Greffet, J. Appl. Phys. **100**, 063704 (2006).

[3] A. Lenert, D.M. Bierman, Y. Nam, W.R. Chan, I. Celanovic, and E.N. Wang, Nat. Nanotechnol. **9**, 126 (2014).

[4] B. Zhao, P. Santhanam, K. Chen, S. Buddhiraju, and S. Fan, Nano Lett. **18**, 5224 (2018).

[5] Z. Wang, Z.M. Zhang, X. Quan, and P. Cheng, Sol. Energy **159**, 329 (2018).

[6] S. Molesky and Z. Jacob, Phys. Rev. B **91**, 205435 (2015).

[7] A. Tittl, A.-K.U. Michel, M. Schäferling, X. Yin, B. Gholipour, L. Cui, M. Wuttig, T. Taubner, F. Neubrech, and H. Giessen, Adv. Mater. **27**, 4597 (2015).

[8] J. Li, J. Wuenschell, Y. Jee, P.R. Ohodnicki, and S. Shen, Phys. Rev. B **99**, 235414 (2019).

[9] J. Kou, Z. Jurado, Z. Chen, S. Fan, and A.J. Minnich, ACS Photonics **4**, 626 (2017).

[10] L. Zhu, A. Raman, K.X. Wang, M.A. Anoma, and S. Fan, Optica **1**, 32 (2014).

[11] A.P. Raman, M.A. Anoma, L. Zhu, E. Rephaeli, and S. Fan, Nature **515**, 540 (2014).

[12] P.C. Hsu, A.Y. Song, P.B. Catrysse, C. Liu, Y. Peng, J. Xie, S. Fan, and Y. Cui, Science (80-.). **353**, 1019 (2016).

[13] B. Guha, C. Otey, C.B. Poitras, S. Fan, and M. Lipson, Nano Lett. **12**, 4546 (2012).

[14] P. Yang, C. Chen, and Z.M. Zhang, Sol. Energy **169**, 316 (2018).

[15] C.R. Otey, W.T. Lau, and S. Fan, Phys. Rev. Lett. **104**, (2010).

[16] A. Ott, R. Messina, P. Ben-Abdallah, and S.-A. Biehs, Appl. Phys. Lett. **114**, 163105 (2019).

[17] A. Ghanekar, J. Ji, and Y. Zheng, Appl. Phys. Lett. **109**, 123106 (2016).

[18] Y.H. Kan, C.Y. Zhao, and Z.M. Zhang, Phys. Rev. B **99**, 035433 (2019).

[19] B. Yu, J. Li, and S. Shen, J. Photonics Energy **9**, 1 (2019).

[20] B. Liu, W. Gong, B. Yu, P. Li, and S. Shen, Nano Lett. **17**, 666 (2017).

[21] X. Liu and Z. Zhang, ACS Photonics **2**, 1320 (2015).

[22] B. Liu and S. Shen, Phys. Rev. B **87**, 115403 (2013).

[23] S.-A. Biehs, M. Tschikin, and P. Ben-Abdallah, Phys. Rev. Lett. **109**, 104301 (2012).

[24] J. Shi, B. Liu, P. Li, L.Y. Ng, and S. Shen, Nano Lett. **15**, 1217 (2015).

[25] X. Liu, T. Tyler, T. Starr, A.F. Starr, N.M. Jokerst, and W.J. Padilla, Phys. Rev. Lett. **107**, 045901 (2011).

[26] S. Pendharker, H. Hu, S. Molesky, R. Starko-Bowes, Z. Poursoti, S. Pramanik, N. Nazemifard, R. Fedosejevs, T. Thundat, and Z. Jacob, J. Opt. **19**, 055101 (2017).

[27] Y. Guo, C.L. Cortes, S. Molesky, and Z. Jacob, Appl. Phys. Lett. **101**, 131106 (2012).

[28] B. Liu, J. Li, and S. Shen, ACS Photonics **4**, 1552 (2017).

[29] L. Zhu, S. Sandhu, C. Otey, S. Fan, M.B. Sinclair, and T.S. Luk, Appl. Phys. Lett. **102**, 103104 (2013).

[30] A. Karalis and J.D. Joannopoulos, Appl. Phys. Lett. **107**, 141108 (2015).

[31] E.S.C. Ching, P.T. Leung, A.M. Van Den Brink, W.M. Suen, and S.S. Tong, Rev. Mod. Phys. **70**, 1545 (1998).

[32] C. Sauvan, J.P. Hugonin, I.S. Maksymov, and P. Lalanne, Phys. Rev. Lett. **110**, 237401

(2013).

[33] C. Sauvan, J.P. Hugonin, R. Carminati, and P. Lalanne, Phys. Rev. A **89**, 043825 (2014).

[34] Kittel C, *Introduction to Solid State Physics, 8th Edition, Berkeley* (1996).

[35] J.C. Slater and G.F. Koster, Phys. Rev. **94**, 1498 (1954).

[36] B. Liu, J. Li, and S. Shen, ACS Photonics **4**, 1552 (2017).

[37] M. Zhou, S. Yi, T.S. Luk, Q. Gan, S. Fan, and Z. Yu, Phys. Rev. B **92**, 024302 (2015).

[38] S. Mallawaarachchi, M. Premaratne, S.D. Gunapala, and P.K. Maini, Phys. Rev. B **95**, 155443 (2017).

[39] J. Li, B. Liu, and S. Shen, Phys. Rev. B **96**, 075413 (2017).